ISSN 0965-5425, Computational Mathematics and Mathematical Physics, 2008, Vol. 48, No. 8, pp. 1349–1366. © Pleiades Publishing, Ltd., 2008.
Original Russian Text © Yu.V. Vassilevski, I.V. Kapyrin, 2008, published in Zhurnal Vychislitel'noi Matematiki i Matematicheskoi Fiziki, 2008, Vol. 48, No. 8, pp. 1429–1447.

Two Splitting Schemes for Nonstationary Convection–Diffusion Problems on Tetrahedral Meshes

Yu. V. Vassilevski and I. V. Kapyrin

Institute of Numerical Mathematics, Russian Academy of Sciences, ul. Gubkina 8, Moscow, 119991 Russia
e-mail: vasilevs@dodo.inm.ras.ru, kap-ivan@bk.ru

Received March 2, 2007; in final form, December 12, 2007

Abstract—Two splitting schemes are proposed for the numerical solution of three-dimensional nonstationary convection–diffusion problems on unstructured meshes in the case of a full diffusion tensor. An advantage of the first scheme is that splitting is generated by the properties of the approximation spaces and does not reduce the order of accuracy. An advantage of the second scheme is that the resulting numerical solutions are nonnegative. A numerical study is conducted to compare the splitting schemes with classical methods, such as finite elements and mixed finite elements. The numerical results show that the splitting schemes are characterized by low dissipation, high-order accuracy, and versatility.

DOI: 10.1134/S0965542508080071

Keywords: nonstationary convection–diffusion problem, splitting scheme, tetrahedral meshes, contaminant transport in porous media.

1. INTRODUCTION

The nonstationary convection–diffusion equation underlies the simulation of contaminant transport in porous media (see [1]). Therefore, the design and analysis of efficient numerical schemes for this equation is a key point in the successful solution to many applications. The parameters of real-life problems impose minimal constraints on the diffusion and convection coefficients: the diffusion tensor can be full, anisotropic, and heterogeneous (i.e., it varies from mesh to mesh), while the convective transport field can vary strongly in space. As a result, diffusive processes dominate in some areas of the computational domain, while convective processes prevail in others. If the computational domain has complex geometry and the solution is nonsmooth in some areas (for example, near a source or at the interface of geological layers), unstructured locally refined (possibly anisotropic) meshes have to be used. We employ tetrahedral meshes, which are best suited for the discretization of complex-shaped computational domains and local refinement.

The above-mentioned properties of the coefficients and meshes restrict the class of possible discretizations. For example, well-elaborated finite-difference methods [2] are difficult to apply on unstructured tetrahedral meshes. In our view, the most promising approximations for this class of problems are those based on finite-element methods (FEMs) [3] and finite-volume methods (FVMs), which are addressed below in the context of numerical scheme design.

Traditionally, the design of numerical schemes for the convection–diffusion equation begins with a spatial approximation of the diffusion operator. The simplest and most popular technique for this is the FEM with the space of continuous piecewise linear functions [3]. This method is denoted by P_1-FEM. Its shortcomings include nonmonotonicity on arbitrary unstructured meshes and the lack of approximation of numerical fluxes at cell interfaces. The mixed finite element method (MFEM) [4] simultaneously approximates both the solution and the diffusive fluxes. As applied to diffusion problems, a shortcoming of the MFEM is that it is not monotone on unstructured and anisotropic meshes [5]. The Galerkin method with discontinuous elements (discontinuous Galerkin (DG) [6]) is a modern alternative to the above techniques when flexibility is needed in the specification of the degree of the approximating polynomial for each cell or when the meshes used are not conformal. Since these advantages are not important for the class of problems under consideration, while the behavior of the DG method is similar to the MFEM [7], we do not address this method below.

The FVM is widely used in engineering applications. For unstructured triangulations, the FVM with a two-point diffusive flux approximation imposes considerable constraints on meshes (mesh orthogonality or Delaunay and Voronoi meshes [8]), while the FVM with multipoint flux stencils requires meshes with regular cells [9]. Moreover, the construction of a linear FVM scheme is considerably complicated for a full dif-

fusion tensor. A nonlinear monotone FVM scheme on two-dimensional unstructured triangular meshes for full diffusion tensors was proposed in [10] and was later improved in [11]. Following the idea of this method, a three-dimensional monotone FVM scheme was constructed in [12].

The transition from the diffusion to convection–diffusion problems leads to additional difficulties in the design of stable schemes in the case of dominating convection. First, regularization can be used to stabilize schemes (see [2]). A classical example is P_1-FEM combined with the streamline upwinding Petrov–Galerkin (SUPG) algorithm [13]. In the case of MFEM and FVM, the convective term is approximated by an upwind scheme. Second, the convective operator can be approximated using shock-capturing schemes based on the Godunov [14], Lax and Friedrichs [15], etc., methods. Examples are methods involving discontinuous finite elements (DFEM) [16, 17] and flux correction [18]. The latter technique ensures monotonicity and minimum numerical diffusivity but does not apply to full and heterogeneous diffusion tensors. These methods approximate nonsmooth solutions with low numerical diffusivity without oscillations.

Time stepping in nonstationary convection–diffusion problems can be based on explicit schemes, implicit schemes, or splitting methods [19]. Both explicit and implicit schemes make use of the same spatial approximation of the convection and diffusion terms (FEM, MFEM, or FVM; as applied to a two-dimensional test problem, the methods were compared in [5]). Splitting schemes [16, 17, 20] make it possible to choose the most suitable approximation method for each spatial operator. That is why, in our view, these schemes will underlie promising time-stepping methods for the nonstationary convection–diffusion equation.

Two splitting methods are discussed in detail in this paper. The first was proposed by Jaffre [21], and splitting in it arises only formally from the orthogonality of two subspaces. For this reason, the method has a higher order of accuracy. The idea behind the method is that different approximations are used for the elliptic and hyperbolic parts of the spatial operator. Specifically, an explicit scheme is used for the convective term, and the Crank–Nicholson scheme, for the diffusion term. Diffusive fluxes are determined using the MFEM, while the scalar solution is found by applying DFEM. The second splitting method was developed by the authors. It involves a new nonlinear FVM scheme [12] and is monotone on arbitrary tetrahedral meshes.

This paper is organized as follows. A model convection–diffusion problem is formulated in Section 2. The relevant mesh elements and mesh spaces are defined in Section 3. Two splitting schemes are described in Section 4. In Section 5, these schemes and two implicit methods are compared in terms of their orders of accuracy with classical spatial discretizations for a smooth solution. In Section 6, we estimate the performance of the schemes as applied to concentration front transport and discuss their monotonicity and numerical diffusion.

2. NONSTATIONARY CONVECTION–DIFFUSION PROBLEM

Let Ω be a bounded polyhedral domain in $\mathbb{R}^3$ with a boundary $\partial\Omega$. Consider the following model convection–diffusion problem (for simplicity, with homogeneous Dirichlet boundary conditions):

$$\frac{\partial C}{\partial t} - \nabla \cdot D\nabla C + \mathbf{b} \cdot \nabla C = F \quad \text{in} \quad \Omega \times (0, T], \tag{1a}$$

$$C = 0 \quad \text{on} \quad \partial\Omega \times (0, T], \tag{1b}$$

$$C = C_0(x) \quad \text{in} \quad \Omega \quad \text{at} \quad t = 0. \tag{1c}$$

Here, C is the contaminant concentration, $\mathbf{b} = \mathbf{b}(x)$ is a conservative convective flux field, $F = F(x)$ is the function of sources or sinks, and $D = D(x)$ is a symmetric positive definite 3×3 diffusion tensor.

The mixed formulation of problem (1) is

$$\frac{\partial C}{\partial t} + \nabla \cdot \mathbf{r} - \mathbf{b} \cdot D^{-1}\mathbf{r} = F \quad \text{in} \quad \Omega \times (0, T], \tag{2a}$$

$$\mathbf{r} = -D\nabla C \quad \text{in} \quad \Omega \times (0, T], \tag{2b}$$

$$C = 0 \quad \text{on} \quad \partial\Omega \times (0, T], \tag{2c}$$

$$C = C_0(x) \quad \text{in} \quad \Omega \quad \text{at} \quad t = 0, \tag{2d}$$

where $\mathbf{r}$ is the diffusive flux. The finite-element discretizations are based on weak formulations [22, 4] of problems (1) and (2).

3. TETRAHEDRAL MESH AND MESH SPACES

Let a conformal tetrahedral mesh ε_h be introduced in the computational domain Ω. Denote the mesh cells by E_i, $i = 1, 2, \ldots, N_E$; the nodes by $O_i = (x_i, y_i, z_i)$, $i = 1, 2, \ldots, N_P$; and the cell interfaces by f_i, $i = 1, 2, \ldots, N_F$. The index sets for internal and boundary nodes are denoted by $\mathcal{N}_I$ and $\mathcal{N}_B$, respectively. Similarly, the index set for cell interfaces is divided into internal and boundary subsets $\mathcal{F}_I$ and $\mathcal{F}_B$. For any set $\mathcal{A}$, the number of its elements is designated as $N_{\mathcal{A}}$. The set of all cell interfaces is denoted by $\partial\varepsilon_h$.

To construct approximating schemes, we need finite-element spaces. Specifically, we define the space of discontinuous piecewise linear functions on ε_h

$$W_h = \{v \in L_2(\Omega),\ v|_E \in P_1(E),\ v|_{\partial E \cap \partial\Omega} = 0\ \forall E \in \varepsilon_h\};$$

the space of piecewise constant functions on ε_h

$$L_h = \{v \in L_2(\Omega),\ v|_E \in P_0(E)\ \forall E \in \varepsilon_h\};$$

the space of piecewise constant functions on $\partial\varepsilon_h$

$$\Lambda_h = \{\lambda \in L_2(\partial\varepsilon_h),\ v|_f \in P_0(f)\ \forall f \in \partial\varepsilon_h\};$$

the lowest order Raviart–Thomas space of fluxes

$$R_h = \{\mathbf{r} \in H(\mathrm{div}, \Omega),\ \mathbf{r}|_E \in RT_0(E)\ \forall E \in \varepsilon_h\};$$

and the space of discontinuous fluxes

$$\tilde{R}_h = \{\mathbf{r} \in (L_2(\Omega))^3,\ \mathbf{r}|_E \in RT_0(E)\ \forall E \in \varepsilon_h\};$$

where

$$RT_0(E) = \left\{\mathbf{r} \in (P_1(E))^3,\ \mathbf{r} = \begin{pmatrix} a + dx \\ b + dy \\ c + dz \end{pmatrix},\ a, b, c, d \in \mathbb{R}\right\}.$$

The constraint $R_h \subset H(\mathrm{div}, \Omega)$ [4] means that the normal component of a vector function from R_h is continuous at any internal cell interface. The basis functions of R_h are linear inside the tetrahedra and have a unit flux through one of the cell interfaces and a zero flux through the others. The basis functions in W_h, Λ_h, and $\tilde{R}_h$ are specified over elements (or cell interfaces) since there are no continuity constraints.

4. DISCRETIZATION METHODS FOR THE PROBLEM

Consider two splitting schemes for approximating Eq. (1): Jaffre's scheme, which uses DFEM for the convection operator and MFEM for the diffusion operator (a brief presentation can be found in [21]), and a new splitting scheme with a monotone FVM approximation of the diffusion operator and DFEM for the convection operator.

4.1. Jaffre's Scheme: DFEM for the Convection Operator and MFEM for the Diffusion Operator

At every time step, Jaffre's scheme computes finite-element approximations of the concentration $C_h^{n+1} \in W_h$ and the diffusive fluxes $\mathbf{r}_h^{n+1} \in R_h$. A single step of the scheme consists of three substeps:

I.

$$\int_E \frac{C_h^{n+\frac{1}{2}} - C_h^n}{\Delta t/2} w_h dx + \int_E \left(\frac{3}{2}\nabla \cdot \mathbf{r}_h^n - \frac{1}{2}\nabla \cdot \mathbf{r}_h^{n-1}\right) w_h dx - \int_E \mathbf{b} C_h^n \cdot \nabla w_h dx + \int_{\partial E} \mathbf{b} C_{h,\,\mathrm{in}}^n \cdot \mathbf{n} w_h ds = \int_E F^n w_h dx \quad \forall w_h \in W_h(E), \quad \forall E \in \varepsilon_h; \tag{3a}$$

II.

$$\int_E \frac{C_h^* - C_h^n}{\Delta t} w_h dx + \int_E \left(\frac{\nabla \cdot \mathbf{r}_h^n + \nabla \cdot \mathbf{r}_h^{n+1}}{2} \right) w_h dx - \int_E \mathbf{b} C_h^{n+\frac{1}{2}} \cdot \nabla w_h dx$$
$$+ \int_{\partial E} \mathbf{b} C_{h,\,\text{in/out}}^{n+\frac{1}{2}} \cdot \mathbf{n} w_h ds = \int_E F^{n+\frac{1}{2}} w_h dx \quad \forall w_h \in W_h(E), \quad \forall E \in \varepsilon_h, \tag{3b}$$

$$\int_\Omega D^{-1} \left(\frac{\mathbf{r}_h^n + \mathbf{r}_h^{n+1}}{2} \right) \cdot \mathbf{q}_h dx - \int_\Omega \left(\frac{C_h^n + C_h^*}{2} \right) \nabla \cdot \mathbf{q}_h dx = 0 \quad \forall \mathbf{q}_h \in R_h; \text{ and} \tag{3c}$$

III.

$$C_h^{n+1} : C_E^{n+1} = \arg \min_{C_E \in P_E \cap Q_E} J(C_E) \quad \forall E \in \varepsilon_h,$$
$$J(C_E) = \frac{1}{2} \sum_{i=1}^4 (C_{E,i} - C_{E,i}^*)^2. \tag{3d}$$

Here, $W_h(E)$ is the restriction of W_h to the tetrahedron E; $\mathbf{n}$ is the outward unit normal to ∂E; C_E^* (C_E^{n+1}) is the vector of the values C_h^* (respectively, C_h^{n+1}) at the vertices of E, i.e., $C_E^* = (C_{E,1}^*, C_{E,2}^*, C_{E,3}^*, C_{E,4}^*)$;

$$P_E = \left\{ C \in \mathbb{R}^4 \Big| \sum_{i=1}^4 c_i = 4 \overline{C}_E^* \right\},$$

where $\overline{C}_E^* = \sum_{i=1}^4 C_{E,i}^*/4$ is the mean of C_h^* on E; and $Q_E = \prod_{i=1}^4 [\min(i), \max(i)]$, where $\min(i)$ and $\max(i)$ are the respective minimum and maximum values of $\overline{C}_{E'}^*$ over all the tetrahedra E' containing the ith vertex of E.

At predictor step (3a), the intermediate concentration $C_h^{n+1/2}$ is explicitly calculated, which is then used in (3b) and (3c) to determine the convective terms. Since functions from W_h are discontinuous at the cell interfaces f_i ($i \in \mathcal{F}_l$), we must specify what we mean by the trace of a function on each cell interface. In the integral over ∂E, $C_{h,\,\text{in}}^n$ is the concentration at the element E. At step (3b), (3c), the convection operator is approximated by an explicit scheme in time, while the Crank–Nicholson scheme is used for the diffusion operator. Moreover, we apply an upwind approximation in the convective term in order to make the scheme stable; i.e., $C_{h,\,\text{in/out}}^{n+1/2}$ in the integral over a cell interface is taken on the tetrahedron on which the convective flux in the outward normal direction to that interface is positive.

After steps (3a)–(3c) are performed, a slope-limiting procedure [24, 25] in the form of minimization problem (3d) is applied to the resulting solution C_h^*. This problem is solved as follows.

Introducing a Lagrange multiplier μ, we pass to the dual formulation of minimization problem (3d): find $(C_E^{n+1}, \lambda) \in Q_E \times \mathbb{R}$ such that

$$\mathcal{L}(C_E^{n+1}, \lambda) = \max_{\mu \in \mathbb{R}} \min_{V \in Q_E} \mathcal{L}(V, \mu), \quad \mathcal{L}(V, \mu) = J(V) - \mu \left[\sum_{i=1}^4 V_i - 4 \overline{C}_E^* \right]. \tag{4}$$

Denote by $\mathcal{P}$ the projector of the vector C_E onto the hypercube Q_E. For fixed μ, the minimization problem

$$V(\mu) = \arg \min_{V \in Q_E} \mathcal{L}(V, \mu)$$

is solved by $V(\mu) = \mathcal{P}(C_E^* + \mu e)$, where $e = (1, 1, 1, 1)$, since

$$\mathcal{L}(V, \mu) = \frac{1}{2}\|V - (C_E^* + \mu e)\|^2 - \frac{\mu^2}{2}\|e\|^2.$$

Instead of solving the maximization problem in (4), we use the properties of $V(\mu)$ and describe a simpler method for finding λ. Note that $F(\mu) = \overline{V(\mu)} - \overline{C}_E^*$ is a continuous, piecewise linear, and monotone function. Therefore, the equation $F(\mu) = 0$ has the unique solution λ, which is to be found. The derivative $F'(\mu)$ is discontinuous at points of the form $\{d_i = C_{E,i}^* - \max(i)\}_{i=1}^4$ and $\{d_i = C_{E,i-4}^* - \min(i-4)\}_{i=5}^8$. Arranging all d_i in ascending order, we see that $F(\mu)$ is linear, monotone increasing, and continuous at the points d_i on the intervals $[d_i, d_{i+1}]$. Let $\sigma_i = F(d_i)$. Since problem (3d) is well-posed, there exists i for which $\sigma_i \le 0$ and $\sigma_{i+1} \ge 0$. Recovering the linear function $F(\mu)$ on $[d_i, d_{i+1}]$, we find the desired solution to the problem:

$$\mu = \frac{d_i\sigma_{i+1} - d_{i+1}\sigma_i}{\sigma_{i+1} - \sigma_i},$$

$$C_{E,i}^{n+1} = (\mathcal{P}(C_E^* + \mu e))_i = \begin{cases} \min(i) & \text{at} \quad C_{E,i}^* + \mu \le \min(i), \\ \max(i) & \text{at} \quad C_{E,i}^* + \mu \ge \max(i), \\ C_{E,i}^* + \mu & \text{outherwise}. \end{cases} \tag{5}$$

Let us return to Jaffre's scheme. Step (3b), (3c) is implemented using the orthogonal decomposition $W_h(E) = W_h(E) = L_h(E) \oplus \tilde{W}_h^1(E)$, where $L_h(E)$ is the space of constants on E and $\tilde{W}_h^1(E)$ is the space of linear functions on E with a zero mean. Then, the second step splits into two substeps:

IIa.

$$\int_E \frac{\overline{C}_h^* - \overline{C}_h^n}{\Delta t} w_h dx + \int_E \left(\frac{\nabla \cdot \mathbf{r}_h^n + \nabla \cdot \mathbf{r}_h^{n+1}}{2}\right) w_h dx + \int_{\partial E} \mathbf{b} C_{h,\text{in/out}}^{n+1/2} \cdot \mathbf{n} w_h ds = \int_E F^{n+\frac{1}{2}} w_h dx \tag{6a}$$
$$\forall w_h \in L_h(E), \quad \forall E \in \varepsilon_h,$$

$$\int_\Omega D^{-1}\left(\frac{\mathbf{r}_h^n + \mathbf{r}_h^{n+1}}{2}\right)\mathbf{q}_h dx - \int_\Omega \left(\frac{\overline{C}_h^n + \overline{C}_h^*}{2}\right)\nabla \cdot \mathbf{q}_h dx = 0 \quad \forall \mathbf{q}_h \in R_h; \tag{6b}$$

IIb.

$$\int_E \frac{\tilde{C}_h^* - \tilde{C}_h^n}{\Delta t} \tilde{w}_h dx - \int_E \mathbf{b} C_h^{n+1/2} \cdot \nabla \tilde{w}_h dx + \int_{\partial E} \mathbf{b} C_{h,\text{in/out}}^{n+1/2} \cdot \mathbf{n} \tilde{w}_h ds = \int_E F^{n+\frac{1}{2}} \tilde{w}_h dx \tag{6c}$$
$$\forall \tilde{w}_h \in \tilde{W}_h^1(E), \quad \forall E \in \varepsilon_h.$$

Here, $\tilde{C}_h^*$ and $\tilde{C}_h^n$ are the linear components of C_h^* and C_h^n that are orthogonal to a constant, while $\overline{C}_h^n$ and $\overline{C}_h^*$ are the means of C_h^n and C_h^* on the tetrahedron. By the definition of R_h, no diffusive fluxes are involved in (6c). Step (6c) is executed locally over tetrahedra possibly using the data from neighboring tetrahedra ($C_{h,\text{in/out}}^{n+1/2}$).

System (6a), (6b) is the standard formulation of the MFEM. Replacing R_h by $\tilde{R}_h$ and introducing Lagrange multipliers $\lambda_h \in \Lambda_h$, we obtain a hybrid formulation of step (6a), (6b): find $(\overline{C}_h^*, \mathbf{r}_h^{n+1}, \lambda_h^{n+1}) \in L_h \times \tilde{R}_h \times \Lambda_h$ for which

$$\int_E \frac{\overline{C}_h^* - \overline{C}_h^n}{\Delta t} w_h dx + \int_E \frac{\nabla \cdot \mathbf{r}_h^n + \nabla \cdot \mathbf{r}_h^{n+1}}{2} w_h dx + \int_{\partial E} \mathbf{b} C_{h,\text{in/out}}^{n+1/2} \cdot \mathbf{n} w_h ds = \int_E F^{n+\frac{1}{2}} w_h dx \tag{7a}$$
$$\forall w_h \in L_h(E), \quad \forall E \in \varepsilon_h,$$

$$\int_E D^{-1}\frac{\mathbf{r}_h^{n+1}+\mathbf{r}_h^n}{2}\cdot\mathbf{q}_h dx-\int_E\frac{\overline{C}_h^n+\overline{C}_h^*}{2}\nabla\cdot\mathbf{q}_h dx+\int_{\partial E\setminus\partial\Omega}\frac{\lambda_h^{n+1}+\lambda_h^n}{2}\mathbf{q}_h\cdot\mathbf{n}ds=0\quad\forall\mathbf{q}_h\in\tilde{R}_h(E),\quad\forall E\in\varepsilon_h,\tag{7b}$$

$$\sum_{E\in\varepsilon_h}\int_{\partial E\setminus\partial\Omega}\mathbf{r}_h^{n+1}\cdot\mathbf{n}\mu_h ds=0\quad\forall\mu_h\in\Lambda_h.\tag{7c}$$

The algebraic system generated by Eqs. (7) becomes (see [4])

$$\mathrm{A}r^{n+1}+\mathrm{B}c^*+\mathrm{C}\lambda^{n+1}=F_1,\tag{8a}$$

$$\mathrm{B}^{\mathrm{T}}r^{n+1}-\mathrm{G}c^*=F_2,\tag{8b}$$

$$\mathrm{C}^{\mathrm{T}}r^{n+1}=0,\tag{8c}$$

where r^{n+1} is the expansion of $\mathbf{r}_h^{n+1}$ over the basis of $\tilde{R}_h(E)$, c^* and λ^{n+1} are the vectors of $\overline{C}_h^*$ and λ_h^{n+1} in cells and at cell interfaces, and F_1 and F_2 contain all the terms involving the source $F^{n+1/2}$ and the values from the time levels n and $n+1/2$. Let A_E, B_E, and G_E denote the restrictions of the matrices A, B, and G to the element E. The elements of A_E and B_E are defined in terms of the basis functions $\mathbf{q}_{E,i}\in\tilde{R}_h(E)$, $i=1,2,3,4$:

$$(A_E)_{ij}=(D^{-1}\mathbf{q}_{E,i},\mathbf{q}_{E,j})_E,\quad(B_E)_i=-(1,\nabla\cdot\mathbf{q}_{E,i})_E,\quad G_E=\left(1,\frac{1}{\Delta t}\right)_E.$$

Here and below, $(\cdot,\cdot)_S$ denotes the inner product in $L_2(S)$, S is a subdomain of $\mathbb{R}^3$, and $(\cdot,\cdot)\equiv(\cdot,\cdot)_\Omega$. The matrix C^{T} in (8c) is responsible for the continuity of the diffusive fluxes $\mathbf{r}_h^{n+1}$ through the cell interfaces f_i, $i\in\mathcal{F}_I$. It is formed by assembling the local components whose elements are expressed by the formula

$$(\mathrm{C}_E)_{ij}=(1,\mathbf{q}_{E,i}\cdot\mathbf{n}_{E,j})_{f_{E,j}},$$

where $f_{E,j}$ is the jth face of E, and $\mathbf{n}_{E,j}$ is the outward unit normal to $f_{E,j}$ with respect to E. Grid equations (7a) and (7b) are formed separately on each tetrahedron and do not involve any variables from other elements. Therefore, (8a) and (8b) result from the assembly of local MFEM systems. Some of the unknowns are eliminated from linear system (8a)–(8c). First, since A is a positive definite block matrix, we can eliminate r^{n+1}:

$$B^{\mathrm{T}}A^{-1}(F_1-\mathrm{B}c^*-\mathrm{C}\lambda^{n+1})-\mathrm{G}c^*=F_2,\tag{9a}$$

$$C^{\mathrm{T}}\mathrm{A}^{-1}(F_1-\mathrm{B}c^*-\mathrm{C}\lambda^{n+1})=0.\tag{9b}$$

Second, since $B^{\mathrm{T}}A^{-1}B$ is a block diagonal matrix, we can eliminate c^*:

$$\begin{aligned}&[C^{\mathrm{T}}A^{-1}C-C^{\mathrm{T}}A^{-1}B(B^{\mathrm{T}}A^{-1}B+G)^{-1}B^{\mathrm{T}}A^{-1}\mathrm{C}]\lambda^{n+1}\\&=C^{\mathrm{T}}A^{-1}F_1+C^{\mathrm{T}}A^{-1}B(B^{\mathrm{T}}A^{-1}B+G)^{-1}(F_2-B^{\mathrm{T}}A^{-1}F_1).\end{aligned}\tag{10}$$

The elimination of the unknowns is elementwise on each tetrahedron. The resulting system has a positive definite symmetric matrix of order $N_{\mathcal{F}_I}$. It is solved by the conjugate gradient method with the ILU2 preconditioner [23] (modified incomplete second-order factorization with two thresholds). After λ^{n+1} is determined by (10), the mean concentrations and the fluxes are locally recovered by the formulas

$$c^*=-(B^{\mathrm{T}}A^{-1}B+G)^{-1}(F_2-B^{\mathrm{T}}A^{-1}F_1+B^{\mathrm{T}}A^{-1}\mathrm{C}\lambda^{n+1}),\tag{11a}$$

$$r^{n+1}=A^{-1}(F_1-Bc^*-C\lambda^{n+1}).\tag{11b}$$

An important feature of this scheme is that splitting with respect to physical processes is only a method for solving Eqs. (3b) and (3c). Therefore, no additional approximation error is introduced into the method, and it can be regarded as second-order accurate in time and space.

Note that the above decomposition of $W_h(E)$ is not possible on tetrahedra having points on a boundary with Dirichlet conditions. In this case, steps (6a)–(6c) are formally executed, while the boundary of the

domain is divided into two parts: $\partial\Omega = \partial\Omega^{\text{in}} \cup \partial\Omega^{\text{out}}$, where $\partial\Omega^{\text{in}} = \{f_i,\ i \in \mathcal{F}_B : \mathbf{b}\cdot\mathbf{n}_{f_i} < 0\}$ and $\partial\Omega^{\text{out}} = \{f_i, i \in \mathcal{F}_B : \mathbf{b}\cdot\mathbf{n}_{f_i} \geq 0\}$; here, $\mathbf{n}_{f_i}$ is the outward normal to $\partial\Omega$. The boundary conditions are strictly satisfied on $\partial\Omega^{\text{in}}$, while on $\partial\Omega^{\text{out}}$ they are satisfied only in the sense of mean face concentrations $\lambda_h \in \Lambda_h$. Numerical experiments confirm the efficiency and stability of this treatment of the boundary conditions.

4.2. Splitting Scheme: DFEM for the Convection Operator and Monotone FVM for the Diffusion Operator

As in the previous scheme, the concentration is approximated by piecewise linear discontinuous functions from W_h. The scheme involves splitting over physical components, and the diffusion and convection operators are handled at different substeps. More specifically, at each substep, we solve the incomplete equation (see [20, 19])

I.

$$\int_E \frac{C_h^{n+1/2} - C_h^n}{\Delta t/2} w_h dx - \int_E \mathbf{b} C_h^n \cdot \nabla w_h dx + \int_{\partial E} \mathbf{b} C_{h,\text{in}}^n \cdot \mathbf{n} w_h ds = \int_E F^n w_h dx \quad \forall w_h \in W_h(E), \quad \forall E \in \varepsilon_h; \tag{12a}$$

II.

$$\int_E \frac{C_h^{*\text{ad}} - C_h^n}{\Delta t} w_h dx - \int_E \mathbf{b} C_h^{n+\frac{1}{2}} \cdot \nabla w_h dx + \int_{\partial E} \mathbf{b} C_{h,\text{in/out}}^{n+\frac{1}{2}} \cdot \mathbf{n} w_h ds = \int_E F^{n+1/2} w_h dx \tag{12b}$$
$$\forall w_h \in W_h(E), \quad \forall E \in \varepsilon_h;$$

III.

$$C_h^{n+1,\text{ad}}:\ C_E^{n+1,\text{ad}} = \arg \min_{C_E \in P_E \cap Q_E} J(C_E) \quad \forall E \in \varepsilon_h,$$
$$J(C_E) = \frac{1}{2}\sum_{i=1}^{4} (C_{E,i} - C_{E,i}^{*,\text{ad}})^2; \tag{12c}$$

IV.

$$\int_E \frac{\overline{C}_{h,E}^{n+1} - \overline{C}_{h,E}^{n+1,\text{ad}}}{\Delta t} dx = -\sum_{i=1}^{4} r_{E,i}^{n+1} = -\int_{\partial E} \mathbf{r}_E^{n+1} \cdot \mathbf{n} ds \quad \forall E \in \varepsilon_h; \text{ and} \tag{12d}$$

V.

$$C_h^{n+1} = C_h^{n+1,\text{ad}} + (\overline{C}_h^{n+1} - \overline{C}_h^{n+1,\text{ad}}). \tag{12e}$$

The convection operator is approximated by an explicit predictor–corrector scheme with an upwind regularization in the corrector. The intermediate concentration $C_h^{n+1/2}$ is calculated in predictor (12a), while $C_h^{*,\text{ad}}$ in the corrector is calculated from the convective fluxes at the intermediate time level. In the integral over the boundary, $C_{h,\text{in/out}}^{n+1/2}$ is taken on the tetrahedron lying upstream. The slope-limiting procedure (12c), which is similar to (3d), is applied to $C_h^{*,\text{ad}}$. Next, implicit scheme (12d) is used to calculate the addition to the mean concentration due to the diffusive fluxes $r_{E,i}^{n+1}$ through the ith faces of E. The values of $\overline{C}_h^{n+1}$ and $r_{E,i}^{n+1}$ are determined by the nonlinear finite-volume method (NFMON) [12]. Its goal is to derive as sparse a monotone approximation matrix as possible by forming two-point diffusive flux approximations. Then, the solution $\overline{C}_h^{n+1}$ remains nonnegative for nonnegative $\overline{C}_h^{n+1,\text{ad}}$. The idea of the two-dimensional NFMON for diffusion problems was set forth in [10]. The method was improved in [11], since the treatment of the case of an anisotropic diffusion tensor in [10] suffered from a flaw: the approximation matrix of the diffusion operator could be nonmonotone for certain two-dimensional mesh geometry. In this paper, the NFMON in three dimensions [12] is applied to convection–diffusion problems. The geometric constructions pre-

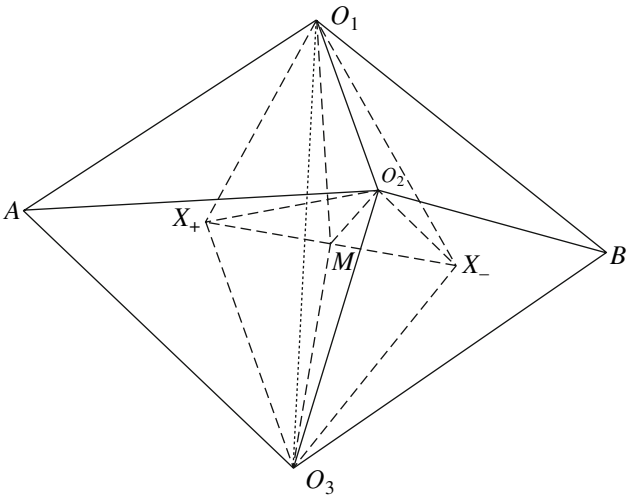

Fig. 1.

sented below guarantee that the approximation matrix of the diffusion operator is monotone for arbitrary tetrahedral meshes and heterogeneous diffusion tensors.

First, we formulate the method for an isotropic homogeneous diffusion tensor D. Let $\mathbb{B} = \{X_j\}_{j=1}^{N_E + N_{\mathcal{F}_B}}$ be the set of collocation points of the degrees of freedom for the discrete concentration. The set $\mathbb{B}$ includes the centers of the inscribed spheres for each tetrahedron and the centers of mass of the external faces f_i, $i \in \mathcal{F}_B$. For each vertex O_i, $i \in \mathcal{N}_I$, there exist four points $X_{i,j}$ ($j = 1, 2, 3, 4$) in $\mathbb{B}$ such that O_i lies inside the tetrahedron formed by them (the nearest points are picked). Therefore, there exist nonnegative coefficients $\lambda_{i,j}$ satisfying the conditions

$$\sum_{j=1}^{4} \lambda_{i,j} \overrightarrow{O_i X_{i,j}} = 0, \quad \sum_{j=1}^{4} \lambda_{i,j} = 1.$$

The coefficients $\lambda_{i,j} \geq 0$ are used for linear interpolation of the concentration at the nodes of the original mesh given its values at the points of $\mathbb{B}$:

$$C_{O_i} = \sum_{j=1}^{4} \lambda_{i,j} C_{X_{i,j}}. \tag{13}$$

Consider the following geometric constructions for the NFMON: two neighboring tetrahedra $T_+ = AO_1O_2O_3$ and $T_- = BO_1O_2O_3$ in the original mesh ε_h (see Fig. 1) and the corresponding elements X_+ and X_- from $\mathbb{B}$ (the centers of inscribed spheres). We introduce the following notation (here and below, i, j, and k are assumed to be different; i.e., $\{i, j, k\} = \{1, 2, 3\}, \{2, 1, 3\}, \{3, 1, 2\}$):

$\mathbf{n}_a$ is the normal to the common face $O_1O_2O_3$ directed from T_+ to T_-.

T_i is the tetrahedron $X_+X_-O_jO_k$.

V_i is the volume of T_i, $i = 1, 2, 3$.

$\mathbf{n}_{ij}$ is the normal to the interface between T_i and T_j directed from T_i to T_j.

$\mathbf{n}_i^+$ ($\mathbf{n}_i^-$) is the outward normal to the faces containing the vertices X_+ (X_-), O_j, and O_k.

The lengths of all the normals are equal to the areas of the corresponding faces.

The diffusive flux $\mathbf{r}_i$ on each tetrahedron T_i is defined using the Green's identity

$$\int_{T_i} \nabla C dx = \int_{\partial T_i} C\mathbf{n} ds.$$

Integrating it to second-order accuracy and taking into account $\mathbf{n}_i^+ + \mathbf{n}_i^- + \mathbf{n}_{ij} + \mathbf{n}_{ik} = 0$, we obtain

$$V_i D^{-1}\mathbf{r}_i = \frac{1}{3}(\mathbf{n}_i^+ C_{X_-} + \mathbf{n}_i^- C_{X_+} + \mathbf{n}_{ij} C_{O_j} + \mathbf{n}_{ik} C_{O_k}). \tag{14}$$

Flux (14) is determined in terms of the concentrations C_{X_+} and C_{X_-} at the points X_+, X_-, as well as at C_{O_j}, and C_{O_k}, for which linear interpolation (13) is used. The total diffusive flux $\mathbf{r}\cdot\mathbf{n}_a$ through $O_1O_2O_3$ is represented as a linear combination of three fluxes $\mathbf{r}_i\cdot\mathbf{n}_a$:

$$\mathbf{r}\cdot\mathbf{n}_a = \mu_1\mathbf{r}_1\cdot\mathbf{n}_a + \mu_2\mathbf{r}_2\cdot\mathbf{n}_a + \mu_3\mathbf{r}_3\cdot\mathbf{n}_a. \tag{15}$$

The expression for μ_i is derived by analogy with the two-dimensional case [10]:

$$\mu_i = \frac{C_{O_i}V_i}{\sum_{j=1}^{3} C_{O_j}V_j}, \quad i = 1, 2, 3. \tag{16}$$

Formula (16) yields the following properties of diffusive flux (15) through $O_1O_2O_3$:

(i) If the values $\mathbf{r}_i\cdot\mathbf{n}_a/|\mathbf{n}_a|$ approximate the diffusive flux density, then $\mathbf{r}\cdot\mathbf{n}_a/|\mathbf{n}_a|$ is also its approximation:

$$\sum_{j=1}^{3}\mu_j = 1. \tag{17}$$

(ii) The approximation stencil for the flux is two-point:

$$\mathbf{r}\cdot\mathbf{n}_a = g_+(C_{O_1}, C_{O_2}, C_{O_3})C_{X_+} - g_-(C_{O_1}, C_{O_2}, C_{O_3})C_{X_-}. \tag{18}$$

Here, g_+ and g_- are determined by substituting (16) and (14) into (15) and are positive for nonnegative concentrations.

If $O_1O_2O_3$ lies on the domain boundary, the Green's identity on the tetrahedron $X_+O_1O_2O_3$ with the volume V_+ yields the equation

$$V_+ D^{-1}\mathbf{r}_i = \frac{1}{3}(C_{X_+}\mathbf{n}_a + C_{O_1}\mathbf{n}_1^+ + C_{O_2}\mathbf{n}_2^+ + C_{O_3}\mathbf{n}_3^+), \tag{19}$$

where C_{O_i} are known from the boundary conditions.

For an anisotropic diffusion tensor, the algorithm for the formation of $\mathbb{B}$ is different. Consider the tetrahedron $T = O_1O_2O_3O_4$ in the original mesh ε_h. Let $\mathbf{R}_i$ be the position vectors of the vertices O_i, and let $\mathbf{N}_i$ be the outward normals to the faces opposite to O_i with the lengths of the normals equal to the areas of the corresponding faces. Inside T, a point X_T is defined by its position vector

$$\mathbf{R}_{X_T} = \frac{\mathbf{R}_1\|\mathbf{N}_1\|_D + \mathbf{R}_2\|\mathbf{N}_2\|_D + \mathbf{R}_3\|\mathbf{N}_3\|_D + \mathbf{R}_4\|\mathbf{N}_4\|_D}{\|\mathbf{N}_1\|_D + \|\mathbf{N}_2\|_D + \|\mathbf{N}_3\|_D + \|\mathbf{N}_4\|_D}, \tag{20}$$

where $\|\mathbf{N}_i\|_D = \sqrt{(D\mathbf{N}_i, \mathbf{N}_i)}$. For an isotropic tensor, expression (20) gives the coordinates of the inscribed sphere. Each tetrahedron $E_i \in \varepsilon_h$ adds to $\mathbb{B}$ the point X_i defined by (20). The center of mass of each face f_i ($i \in \mathcal{F}_B$) is also added to $\mathbb{B}$. As before, the coefficients μ_i are given by (16).

If the diffusion tensor is heterogeneous (i.e., it varies from tetrahedron to tetrahedron), then the degrees of freedom C_{M_1}, C_{M_2}, and C_{M_3} are introduced at the center of mass M of $O_1O_2O_3$. Let T_i^+ (T_i^-) be the tetrahedron $X_+MO_jO_k$ ($X_-MO_jO_k$, respectively), V_i^+ (V_i^-) be its volume, $\mathbf{r}_i^+$ ($\mathbf{r}_i^-$) be an approximation of the diffusive flux inside this tetrahedron, and D_+ (D_-) be the diffusion tensor in it. Integration by analogy with (14) produces

$$V_i^* D_*^{-1}\mathbf{r}_i^* = \frac{1}{3}(\mathbf{n}_i^* C_{M_i} + \mathbf{n}_{ai}^* C_{X_*} + \mathbf{n}_{ij}^* C_{O_j} + \mathbf{n}_{ik}^* C_{O_k}), \quad i \neq j \neq k. \tag{21}$$

Here, the star means a plus or a minus, $\mathbf{n}_{ai}^*$ is normal to MO_jO_k, $\mathbf{n}_{ij}^*$ is the normal to MX_*O_k, and all the normals are exterior with respect to T_i^*. The lengths of the normals are equal to the areas of the corresponding faces. The additional degrees of freedom C_{M_i} are eliminated by assuming that the normal flux component is continuous: $\mathbf{r}_i^+ \cdot \mathbf{n}_a = \mathbf{r}_i^- \cdot \mathbf{n}_a$. The total flux is again calculated by formula (15), where $\mathbf{r}_i \cdot \mathbf{n}_a = \mathbf{r}_i^+ \cdot \mathbf{n}_a = \mathbf{r}_i^- \cdot \mathbf{n}_a$. The coefficients μ_i satisfying (17) and (18) were computed in [12]:

$$\mu_i = \frac{[(D_-\mathbf{n}_i^-, \mathbf{n}_a)V_i^+ - (D_+\mathbf{n}_i^+, \mathbf{n}_a)V_i^-]C_{O_i}}{\sum_{j=1}^{3}[(D_-\mathbf{n}_j^-, \mathbf{n}_a)V_j^+ - (D_+\mathbf{n}_j^+, \mathbf{n}_a)V_j^-]C_{O_j}}. \tag{22}$$

This choice of μ_i again yields a two-point approximation stencil for the diffusive flux. Thus, for homogeneous and heterogeneous diffusion tensors, the discrete diffusive fluxes are defined by (15), (16), or (22).

To implement step (12c), we find the projection $\hat{c}$ of the solution $C_h^{n+1,\,\mathrm{ad}}$ onto the points of $\mathbb{B}$ and solve the NFMON problem for the desired concentrations $\hat{c}^{\mathrm{diff}}$ at the points of $\mathbb{B}$:

$$(\mathrm{V} + \mathrm{A}(\hat{c}^{\mathrm{diff}})\Delta t)\hat{c}^{\mathrm{diff}} = \mathrm{V}\hat{c}. \tag{23}$$

Here, V is a diagonal matrix of element volumes and $\mathrm{A}(\hat{c}^{\mathrm{diff}})$ is an asymmetric FVM matrix whose elements depend on $\hat{c}^{\mathrm{diff}}$. All the off-diagonal and diagonal nonzero elements of $\mathrm{A}(\hat{c}^{\mathrm{diff}})$ are negative and positive, respectively, for nonnegative $\hat{c}^{\mathrm{diff}}$. Moreover, the transpose $(\mathrm{A}(\hat{c}^{\mathrm{diff}}))^{\mathrm{T}}$ is row diagonally dominant. Therefore, $((\mathrm{A}(\hat{c}^{\mathrm{diff}}))^{\mathrm{T}}$ is an M-matrix and $([(\mathrm{A}(\hat{c}^{\mathrm{diff}}))^{\mathrm{T}}]^{-1})_{ij} \geq 0$. Since $(\mathrm{A}^{-1})^{\mathrm{T}} = (\mathrm{A}^{\mathrm{T}})^{-1}$, the matrix $\mathrm{A}(\hat{c}^{\mathrm{diff}})$ is monotone (see [26]). Nonlinear system (23) is solved by the Picard iteration algorithm

$$(\mathrm{V} + \mathrm{A}(\hat{c}^{\mathrm{diff},\,k})\Delta t)\hat{c}^{\mathrm{diff},\,k+1} = \mathrm{V}\hat{c}$$

with the initial approximation $\hat{c}^{\mathrm{diff},\,0} = \hat{c} \geq 0$. Since the matrix $\mathrm{V} + \mathrm{A}(\hat{c}^{\mathrm{diff},\,k})\Delta t$ is monotone for any nonnegative $\hat{c}^{\mathrm{diff},\,k}$, all the iterative approximations $\hat{c}^{\mathrm{diff},\,k+1}$ are nonnegative as well; i.e., scheme (23) is monotone.

After $\hat{c}^{\mathrm{diff}}$ is determined, we use the formula

$$\overline{C}_{h,E}^{n+1} - \overline{C}_{h,E}^{n+1,\,\mathrm{ad}} = \hat{c}_E^{\mathrm{diff}} - \hat{c}_E \quad \forall E \in \varepsilon_h$$

and find the addition to the mean concentrations due to diffusive fluxes, as required in (12e).

5. NUMERICAL RESULTS FOR PROBLEMS WITH SMOOTH SOLUTIONS

Below, the splitting schemes described above are compared with two implicit approximations of Eq. (1): the implicit BDF scheme for P_1-FEM with SUPG stabilization [13] and the BDF MFEM scheme [4] with an upwind approximation of the convective term.

5.1. Notation

Since the methods described above make use of different function spaces, for each of them, we introduce a norm for evaluating the error in the numerical solution against the analytical solution to the differential problem. For the BDF P_1-FEM scheme with SUPG stabilization, the norms are defined as

$$\|\Delta C\|_2 = \left(\sum_{i=1}^{N_E}\int_E [C_h(x) - C(x)]^2 dx\right)^{1/2},$$

$$\|\Delta C\|_{\infty,P} = \max_{1 \leq i \leq N_P} |C_h(O_i) - C(O_i)|.$$

In the BDF MFEM scheme, the concentration C_h is a piecewise constant function that approximates the mean concentration over an element. For this reason, the norms are defined as

$$\|\Delta C\|_{2,E} = \left(\sum_{i=1}^{N_E} [C_h(E_i) - \bar{C}(E_i)]^2 |E_i|\right)^{1/2},$$

$$\|\Delta C\|_{\infty,E} = \max_{1 \le i \le N_E} |C_h(E_i) - \bar{C}(E_i)|,$$

where $|E_i|$ is the volume of the element $E_i \in \mathfrak{E}_h$, $\bar{C}(E_i)$ is the mean of the analytical solution $C(x)$ on E_i, and $C_h(E_i)$ is the value of C_h on E_i.

In the splitting schemes, the concentration is approximated in the space of piecewise linear functions that are discontinuous on the element boundaries. The norm corresponding to discontinuous piecewise linear functions is defined as

$$\|\Delta C\|_{\infty,P'} = \max_{1 \le i \le N_E} \max_{1 \le j \le 4} |C_h(O_{E_i,j}) - C(O_{E_i,j})|.$$

Here, $O_{E_i,j}$, j is the jth vertex of the tetrahedron E_i; and $C_h(O_{E_i,j})$ is the value of C_h at the point $O_{E_i,j}$ on E_i. Since Jaffre's scheme simultaneously finds a piecewise linear discontinuous concentration and a piecewise constant concentration (with the help of MFEM) approximating the mean value, while estimating the errors in this scheme, we also use the norms $\|\cdot\|_{2,E}$ and $\|\cdot\|_{\infty,E}$. In the DFEM + FVM splitting scheme, in addition to a discontinuous piecewise linear approximation, the finite-volume method approximates the concentration at special points X_T of $\mathbb{B}$. The approximation error at these points is estimated using the norms

$$\|\Delta C\|_{2,\mathbb{B}} = \left(\sum_{i=1}^{N_E} [C_h(X_{T,i}) - C(X_{T,i})]^2 |E_i|\right)^{1/2},$$

$$\|\Delta C\|_{\infty,\mathbb{B}} = \max_{1 \le i \le N_E} |C_h(X_{T,i}) - C(X_{T,i})|.$$

The approximation error in fluxes can be calculated for all the schemes, except for P_1-FEM. For this purpose, we introduce the norms for the approximation errors in diffusive fluxes:

$$\|\Delta r\|_\infty = \max_{1 \le i \le N_F} |\bar{r}_{f_i} - r_{h,f_i}|,$$

$$\|\Delta r\|_2 = \left(\sum_{i=1}^{N_E} |E_i| \sum_{j=1}^{4} (\bar{r}_{E_i,j} - r_{h,E_i,j})^2\right)^{1/2},$$

where $\bar{r}_{f_i}$ ($\bar{r}_{E_i,j}$) is the mean of the normal component of the exact diffusive flux density through the face f_i (the jth face of E_i) and $\bar{r}_{h,f_i}$ ($r_{h,E_i,j}$) is the normal component of the flux density $\mathbf{r}_h$ through the face f_i (the jth face of E_i), which is by definition a constant on this face.

5.2. Diffusion-Dominated Problem

As a solution to the test problem, we considered the function $C(x, y, x, t) = (1 - x^2)\sin(y)e^{-z}\sin(t)$ in the unit cube $\Omega = (0; 1)^3$. Dirichlet conditions were set on the boundary. The convective flux $\mathbf{b} = (0.1; z/10; -y/10)$ was a combination of translational motion in the direction of the abscissa axis and rotation about it. The diffusion tensor $D = I$ was a unit tensor. Three uniform structured meshes were used in the computations. The coarsest of them consisted of 3072 tetrahedra (mesh 1). The other two were obtained by uniformly refining the first and contained 24 576 (mesh 2) and 196 608 (mesh 3) elements, respectively (the mesh size was halved in each refinement procedure). In all the schemes, the time steps used in the tests were 0.025 for mesh 1, 0.0125 for mesh 2, and 0.00625 for mesh 3. The errors were calculated for the solution at the time $T = 1$.

Table 1 shows that the traditional P_1-FEM with SUPG regularization is second-order accurate. For diffusion-dominated problems, the BDF MFEM scheme (Table 2) is second-order accurate for concentrations and first-order accurate for diffusive fluxes. Both schemes are unconditionally stable.

Table 1. Dominating diffusion: BDF FEM with SUPG

Mesh	$\|\Delta C\|_{\infty, P}$	$\|\Delta C\|_2$
1	3.4×10^{-3}	1.6×10^{-3}
2	9.8×10^{-4}	4×10^{-4}
3	3.1×10^{-4}	1×10^{-4}

Table 2. Dominating diffusion: BDF MFEM

Mesh	$\|\Delta C\|_{\infty, E}$	$\|\Delta C\|_{2, E}$	$\|\Delta r\|_\infty$	$\|\Delta r\|_2$
1	1.6×10^{-3}	3.3×10^{-4}	4.6×10^{-2}	1.2×10^{-2}
2	4.7×10^{-4}	8.7×10^{-5}	2.5×10^{-2}	5.8×10^{-3}
3	1.5×10^{-4}	2.2×10^{-5}	1.4×10^{-2}	2.8×10^{-3}

Table 3. Dominating diffusion: Jaffre's scheme

Mesh	$\|\Delta C\|_{\infty, P'}$	$\|\Delta C\|_2$	$\|\Delta C\|_{\infty, E}$	$\|\Delta C\|_{2, E}$	$\|\Delta r\|_\infty$	$\|\Delta r\|_2$
1	6.2×10^{-2}	5×10^{-3}	1.7×10^{-3}	3.3×10^{-4}	4.6×10^{-2}	1.2×10^{-2}
2	2.4×10^{-2}	1.7×10^{-3}	4.7×10^{-4}	8.7×10^{-5}	2.6×10^{-2}	5.8×10^{-3}
3	1.1×10^{-2}	5.2×10^{-4}	1.5×10^{-4}	2.2×10^{-5}	1.5×10^{-2}	2.8×10^{-3}

Table 4. Dominating diffusion: DFEM + FVM

Mesh	$\|\Delta C\|_{\infty, P'}$	$\|\Delta C\|_2$	$\|\Delta C\|_{\infty, \mathbb{B}}$	$\|\Delta C\|_{2, \mathbb{B}}$	$\|\Delta r\|_\infty$	$\|\Delta r\|_2$
1	6.2×10^{-2}	5.3×10^{-3}	5×10^{-3}	1.4×10^{-3}	1.1×10^{-1}	2.8×10^{-2}
2	2.5×10^{-2}	1.8×10^{-3}	1.8×10^{-3}	4×10^{-4}	5.6×10^{-2}	1.3×10^{-2}
3	1.1×10^{-2}	5.6×10^{-4}	5.1×10^{-4}	1.2×10^{-4}	2.8×10^{-2}	6×10^{-3}

The results produced by Jaffre's scheme (Table 3) are very similar to BDF MFEM; i.e., for dominating diffusion, the behavior of the scheme is determined by the use of MFEM for approximating the diffusion operator. It was found that the convergence with respect to the norm $\|\cdot\|_{2, E}$ is quadratic for concentrations and linear for diffusive fluxes.

The method with DFEM for convection and FVM for diffusion exhibited linear convergence for diffusive fluxes and quadratic convergence for concentrations in the special norm $\|\cdot\|_{2, \mathbb{B}}$ (Table 4). In both splitting schemes, the CFL condition is imposed on the time step, since the convection is approximated by an explicit method.

5.3. Convection-Dominated Problem

The computational domain, meshes, time steps, and convective fluxes were the same as in the previous problem. The diffusion tensor $D = 10^{-5}I$ was diagonal and isotropic (spherical). The test function was $C(x, y, z, t) = x^2 \sin(y) e^{-z} \sin(t)$. Its choice is explained by the desire to obtain a nonnegative right-hand side on the discretization of Eq. (1a) in order to verify the monotonicity of the schemes. Recall that only the NFMON guarantees the absence of negative concentrations in this case (although it is unsuitable for problems admitting negative concentrations).

The BDF P_1-FEM scheme with SUPG (Table 5) exhibits the same behavior as in the previous problem, and it is still second-order accurate. On the contrary, the BDF MFEM scheme (Table 6) exhibits linear convergence for concentrations and no convergence for fluxes: the stabilization of the convective term generates numerical diffusion that considerably exceeds the actual one. Jaffre's scheme not only remains second-order accurate for concentrations in the norm $\|\cdot\|_{2, E}$ but also exhibits this property in the norm $\|\cdot\|_2$ (Table 7). The cause is that only convective terms are involved in formula (6), which determines the linear concentration

Table 5. Dominating convection: BDF FEM with SUPG

Mesh	$\|\Delta C\|_{\infty, P}$	$\|\Delta C\|_2$
1	3.9×10^{-3}	9.5×10^{-4}
2	1.4×10^{-3}	2.5×10^{-4}
3	6.5×10^{-4}	6.6×10^{-5}

Table 6. Dominating convection: BDF MFEM

Mesh	$\|\Delta C\|_{\infty, E}$	$\|\Delta C\|_{2, E}$	$\|\Delta r\|_\infty$	$\|\Delta r\|_2$
1	3.5×10^{-2}	4.4×10^{-3}	2×10^{-5}	2×10^{-6}
2	2.7×10^{-2}	2.7×10^{-3}	2.5×10^{-5}	2.2×10^{-6}
3	1.7×10^{-2}	1.5×10^{-3}	3×10^{-5}	2.4×10^{-6}

Table 7. Dominating convection: Jaffre's scheme

Mesh	$\|\Delta C\|_{\infty, P^1}$	$\|\Delta C\|_2$	$\|\Delta C\|_{\infty, E}$	$\|\Delta C\|_{2, E}$	$\|\Delta r\|_\infty$	$\|\Delta r\|_2$
1	1.9×10^{-2}	5.7×10^{-4}	4.3×10^{-3}	2.8×10^{-4}	1×10^{-6}	1.8×10^{-7}
2	8.2×10^{-3}	1.4×10^{-4}	1.9×10^{-3}	6.6×10^{-5}	9.7×10^{-7}	8.3×10^{-8}
3	3.5×10^{-3}	3.6×10^{-5}	8.4×10^{-4}	1.5×10^{-5}	7.8×10^{-7}	3.8×10^{-8}

Table 8. Dominating convection: DFEM + FVM

Mesh	$\|\Delta C\|_{\infty, P^1}$	$\|\Delta C\|_2$	$\|\Delta C\|_{\infty, \mathbb{B}}$	$\|\Delta C\|_{2, \mathbb{B}}$	$\|\Delta r\|_\infty$	$\|\Delta r\|_2$
1	1.1×10^{-2}	5.7×10^{-4}	3×10^{-3}	4×10^{-4}	2.9×10^{-6}	3.8×10^{-7}
2	4.8×10^{-3}	1.4×10^{-4}	8.7×10^{-4}	1×10^{-4}	1.5×10^{-6}	1.8×10^{-7}
3	1.2×10^{-3}	3.7×10^{-5}	2.5×10^{-4}	2.5×10^{-5}	7.6×10^{-7}	8.3×10^{-8}

component. Thus, for pure diffusion problems, only mean concentrations on elements can be approximated to second order accuracy, while, in the case of dominating convection, the method is also capable of constructing piecewise linear approximations of the same order. The same is true of the DFEM + FVM scheme (Table 8) with the norm $\|\cdot\|_{2, E}$ replaced by $\|\cdot\|_{2, \mathbb{B}}$.

5.4. Problem with a Full Diffusion Tensor

As an analytical solution, we used $C(x, y, z, t) = x^2 \sin(y) e^{-z} \sin(t) + 1$. The diffusion tensor was full and anisotropic:

$$D = \begin{pmatrix} 10^{-1} & 10^{-4} & 10^{-3} \\ 10^{-4} & 10^{-1} & 10^{-4} \\ 10^{-3} & 10^{-4} & 10^{-2} \end{pmatrix}.$$

The computational domain, meshes, time steps, and convective fluxes were the same as in the previous problems. The test function was bounded away from zero to guarantee that the numerical solution is nonnegative, as required by the NFMON (the source fails to be positive everywhere in Ω).

Tables 9–12 show that, for concentrations, the order of accuracy of the traditional FEM with SUPG is higher than the first, while the BDF MFEM scheme is first-order accurate. Like the FEM, the splitting schemes are also high-order accurate for concentrations. The schemes computing diffusive fluxes exhibit linear convergence in the norm $\|\Delta r\|_2$.

Table 9. Full diffusion tensor: BDF FEM with SUPG

Mesh	$\|\Delta C\|_{\infty, P}$	$\|\Delta C\|_2$
1	2.7×10^{-3}	1×10^{-3}
2	1.1×10^{-3}	2.6×10^{-4}
3	4.9×10^{-4}	7.8×10^{-5}

Table 10. Full diffusion tensor: BDF MFEM

Mesh	$\|\Delta C\|_{\infty, E}$	$\|\Delta C\|_{2, E}$	$\|\Delta r\|_\infty$	$\|\Delta r\|_2$
1	4.9×10^{-3}	5.9×10^{-4}	5.7×10^{-3}	1.5×10^{-4}
2	1.3×10^{-3}	1.8×10^{-4}	5×10^{-3}	7.1×10^{-4}
3	3.7×10^{-4}	7.8×10^{-5}	2.6×10^{-3}	3.5×10^{-4}

Table 11. Full diffusion tensor: Jaffre's scheme

Mesh	$\|\Delta C\|_{\infty, P'}$	$\|\Delta C\|_2$	$\|\Delta C\|_{\infty, E}$	$\|\Delta C\|_{2, E}$	$\|\Delta r\|_\infty$	$\|\Delta r\|_2$
1	1.6×10^{-2}	1×10^{-3}	4.4×10^{-3}	6.6×10^{-4}	5.5×10^{-3}	1.4×10^{-3}
2	5.1×10^{-3}	3×10^{-4}	1.2×10^{-3}	2×10^{-4}	3×10^{-3}	7×10^{-4}
3	1.5×10^{-3}	1×10^{-4}	3.6×10^{-4}	8.3×10^{-5}	1.5×10^{-3}	3.5×10^{-4}

Table 12. Full diffusion tensor: DFEM + FVM

Mesh	$\|\Delta C\|_{\infty, P'}$	$\|\Delta C\|_2$	$\|\Delta C\|_{\infty, \mathbb{B}}$	$\|\Delta C\|_{2, \mathbb{B}}$	$\|\Delta r\|_\infty$	$\|\Delta r\|_2$
1	2.3×10^{-2}	1.4×10^{-3}	5.3×10^{-3}	1.1×10^{-3}	7.4×10^{-3}	1.8×10^{-3}
2	7.5×10^{-3}	4.5×10^{-4}	1.9×10^{-3}	3.4×10^{-4}	3.8×10^{-3}	8.9×10^{-4}
3	2.9×10^{-3}	1.3×10^{-4}	6.2×10^{-4}	9.7×10^{-5}	1.9×10^{-3}	4.4×10^{-4}

6. NUMERICAL RESULTS FOR CONCENTRATION FRONT PROPAGATION

Consider the front of concentration propagating from a constant source occupying a section on the boundary of the domain $\Omega = (0; 1) \times (-0.5; 0.5) \times (-0.5; 0.5)$. More specifically, the following inhomogeneous boundary conditions are set at $x = 0$:

$$C(0, y, z) = \begin{cases} 1 & \text{if} \quad |y| < 1/4, \quad |z| < 1/4, \\ 0 & \text{otherwise}. \end{cases}$$

The initial concentration is zero in the entire domain Ω, and the convective flux is $\mathbf{b} = (1, 0, 0)$. For the solution to have a sharp front, the diffusion tensor is chosen to be small with respect to convection: $D = 10^{-4}I$.

The analytical solution to this problem in the half-space $x \geq 0$ was found in [27]. Passing to the bounded domain Ω, we set Dirichlet conditions on all its boundaries. The numerical solutions are compared with the analytical one at the time $T = 0.5$ on two meshes (structured and unstructured) with roughly identical mesh sizes (see Fig. 2). The unstructured mesh was obtained from the structured one by adding random values to the coordinates of each interior point. The ordinates of the points were left unchanged in order to make the resulting solutions and the mesh in the plane $y = 0$ more visual.

Figures 2–6 display the exact and approximate solutions at $T = 0.5$ in the plane $y = 0$ for the (a) structured and (b) unstructured meshes. The contour lines correspond to the concentration values 0.2, 0.4, 0.6, 0.8, and 1. All the methods, except for splitting with NFMON, are nonmonotone, so the solution takes negative values (Table 13). Figure 7a shows that FEM with SUPG exhibits strong oscillations and higher numerical diffusion than the DFEM schemes. Since the FEM is strongly dispersive, a concentration contour line corre-

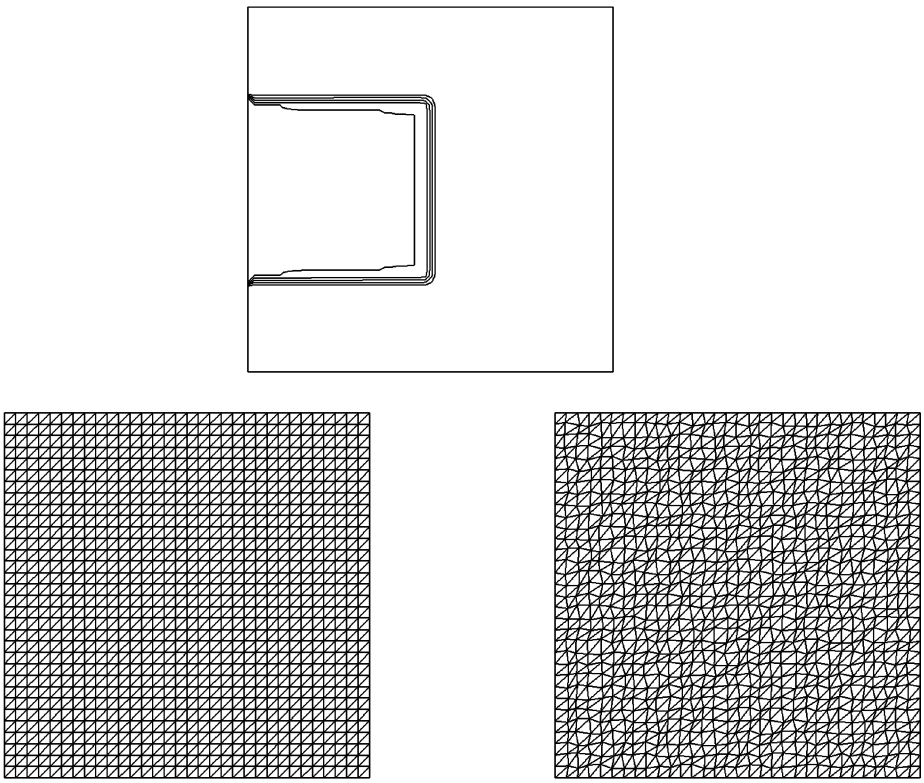

Fig. 2.

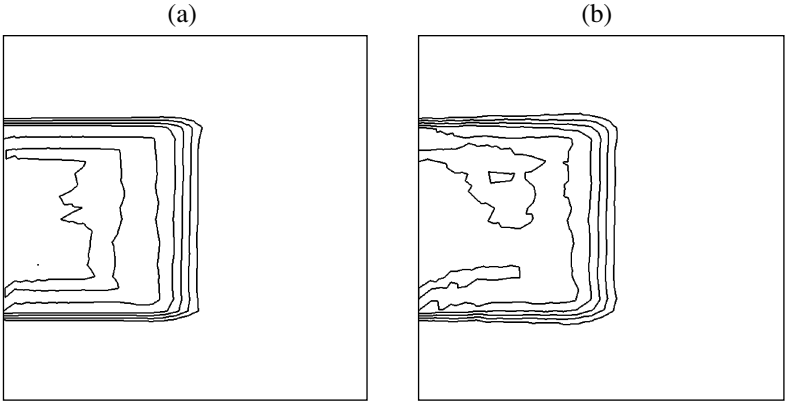

Fig. 3. P_1-FEM+SUPG solution.

sponding to 1 appears in Fig. 3 in the area where the solution must be the identical unit. The MFEM scheme exhibits the highest numerical diffusion, strongly smearing the front (see Fig. 7b). The solutions produced by the splitting schemes are similar, but the DFEM + MFEM solution (Fig. 7c) has small negative concentrations, which are absent from the DFEM + NFMON solution (Fig. 7d). Monotonicity is achieved at the expense of the linearity of the problem, which has to be solved at every time step, thus requiring more CPU time (20% more as compared to Jaffre's scheme). Note that the DFEM + NFMON scheme is unsuitable for negative concentrations, since a positive solution must be obtained at the convective step.

To make the dissipative and dispersion properties of the schemes visual, the analytical and numerical solutions to the problem along the horizontal axis are presented in each panel in Fig. 7. Here, the analytical solution is shown by the solid line, and the numerical solutions on structured and unstructured meshes, by the dotted line with crosses and by circles, respectively. For convection-dominated problems, the plots in

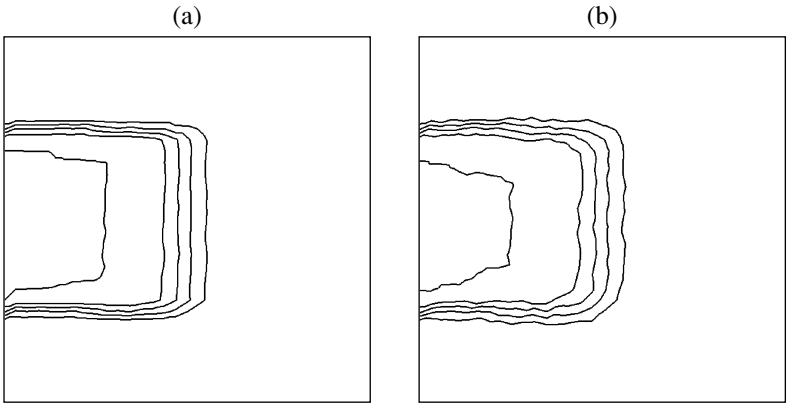

Fig. 4. MFEM solution.

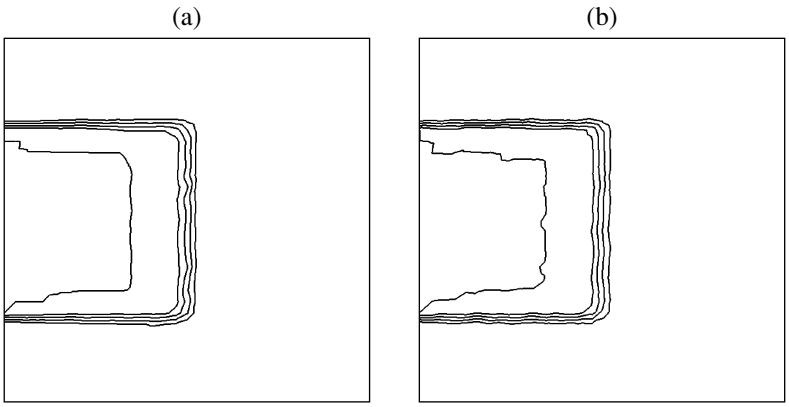

Fig. 5. DFEM + MFEM solution.

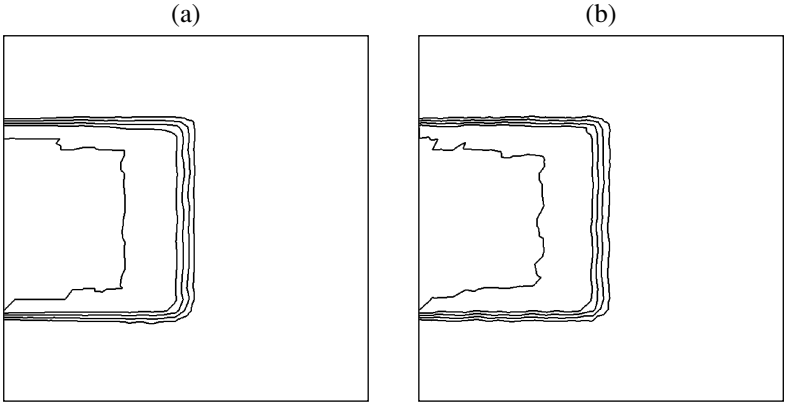

Fig. 6. DFEM + NFMON solution.

Figs. 2–7 reveal that the classical methods are inferior to the new DFEM methods in terms of numerical diffusion and monotonicity. Note that the solutions obtained on structured and unstructured meshes with

Table 13. Minimal mean concentration in the course of the solution

Mesh	FEM	MFEM	DFEM + MFEM	DFEM + FVM
Structured	-1.3×10^{-1}	-5.4×10^{-3}	-1×10^{-2}	0
Unstructured	-1.8×10^{-1}	-6.4×10^{-2}	-6.9×10^{-4}	0

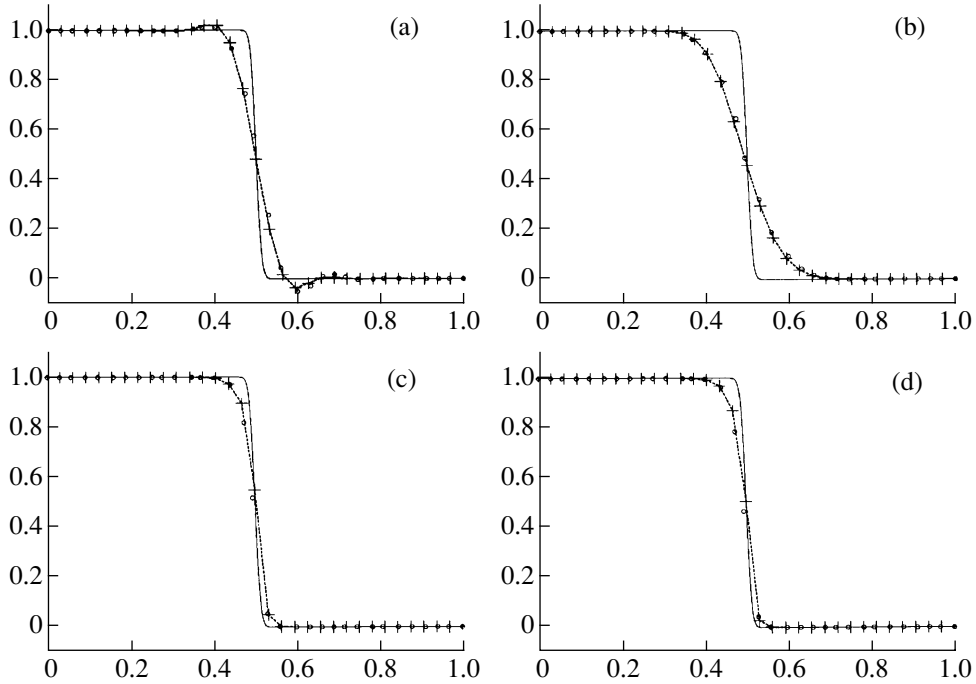

Fig. 7. Analytical and numerical solutions on the line $y = z = 0$.

similar mesh sizes differ little from each other; i.e., the methods are not sensitive to the choice of a mesh.

7. CONCLUSIONS

The analysis of the numerical schemes used in this paper has revealed their strong and weak points as applied to convection–diffusion problems. The traditional implicit linear finite element method with SUPG stabilization was shown to be second-order accurate. However, it fails to approximate diffusive fluxes on cell interfaces. Moreover, in problems with pronounced concentration fronts, it exhibits strong nonmonotonicity, thus being inferior to the splitting schemes in terms of numerical diffusion. The BDF MFEM scheme reveals high-order accuracy for diffusion-dominated problems. However, the method is not recommended for convection-dominated problems, since it exhibits very high numerical diffusion.

The splitting schemes have an order of accuracy higher than the first for concentrations and are first-order accurate for fluxes. They ensure that the mass conservation law holds in each mesh cell. Supplemented with discontinuous finite elements, these methods are most suitable for the simulation of concentration front propagation, in which case they exhibit low numerical diffusion. For problems with a nonsmooth solution, Jaffre's scheme demonstrates only slight violations in monotonicity as compared with the traditional FEM. The new scheme with a nonlinear FVM gives results similar to those produced by Jaffre's scheme and, additionally, is monotone, which is important for applications. However, it becomes unstable in the presence of negative concentrations.

In applications, such as subsurface contaminant transport, the splitting schemes are most suitable, since the media are strongly heterogeneous and possess full diffusion tensors, convective transport dominates in some layers, and the solution can be nonsmooth.

ACKNOWLEDGMENTS

We are grateful to J. Jaffre, K.N. Lipnikov, and D.A. Svyatski for fruitful discussions of the problem. We also thank V.I. Agoshkov for discussing the manuscript and his helpful remarks.

This work was supported in part by the Russian Foundation for Basic Research (project no. 04-07-90336) and by the programs "Computational and Information Issues of the Solution to Large-Scale Problems" and "Optimal Methods for Solving Problems in Mathematical Physics" of the Department of Mathematical Sciences of the Russian Academy of Sciences.

REFERENCES

1. A. Bourgeat, M. Kern, S. Schumacher, and J. Talandier, "The COUPLEX Test Cases: Nuclear Waste Disposal Simulation," Comput. Geosci. **8** (2), 83–98 (2004).
2. A. A. Samarskii and P. N. Vabishchevich, *Numerical Methods for Convection-Diffusion Problems* (Editorial URSS, Moscow, 1999) [in Russian].
3. P. Ciarlet, *The Finite Element Method for Elliptic Problems* (North-Holland, Amsterdam, 1977; Mir, Moscow, 1980).
4. F. Brezzi and M. Fortin, *Mixed and Hybrid Finite Element Methods* (Springer-Verlag, New York, 1991).
5. G. Bernard-Michel, C. Le Potier, A. Beccantini, et. al., "The Andra Couplex 1 Test Case: Comparisons between Finite Element, Mixed Hybrid Finite Element, and Finite Volume Discretizations," Comput. Geosci. **8** (2), 187–201 (2004).
6. *Discontinuous Galerkin Methods: Theory, Computation, and Applications*, Ed. by B. Cockburn, G. E. Karniadakis, and C.-W. Shu (Springer-Verlag, Berlin, 2000).
7. P. Bastian and S. Lang, "Couplex Benchmark Computations Obtained with the Software Toolbox UG," Comput. Geosci. **8** (2), 125–147.
8. I. D. Mishev, "Finite Volume Methods on Voronoi Meshes," Numer. Methods Partial Differ. Equations **12** (2), 193–212 (1998).
9. I. Aavatsmark, T. Barkve, O. Boe, and T. Mannseth, "Discretization on Unstructured Grids for Inhomogeneous, Anisotropic Media. Part I: Derivation of the Methods," SIAM J. Sci. Comput. **19**, 1700–1716 (1998).
10. C. Le Potier, "Schema volumes finis monotone pour des operateurs de diffusion fortement anisotropes sur des maillages de triangle non structures," C.R. Acad. Sci. Paris, Ser. I **341**, 787–792 (2005).
11. K. Lipnikov, M. Shashkov, D. Svyatski, and Yu. Vassilevski, "Monotone Finite Volume Schemes for Diffusion Equations on Unstructured Triangular and Shape-Regular Polygonal Meshes," J. Comput. Phys. **227**, 492–512 (2007).
12. I. V. Kapyrin, "A Family of Monotone Methods for the Numerical Solution of Three-Dimensional Diffusion Problems on Unstructured Tetrahedral Meshes," Dokl. Akad. Nauk **416**, 588–593 (2007) [Dokl. Math. **76**, 734–738 (2007)].
13. T. J. R. Hughes and A. N. Brooks, "A Multidimensional Upwind Scheme with No Crosswind Diffusion," *Finite Element Methods for Convection Dominated Flows* (ASME, New York, 1979), vol. 34, pp. 19–35.
14. S. K. Godunov, "A Difference Method for Numerical Calculation of Discontinuous Solutions of the Equations of Hydrodynamics," Mat. Sb., **47(89)**, 271–306 (1959).
15. P. D. Lax, "Shock Waves and Entropy," in *Contributions to Nonlinear Functional Analysis* (Academic, New York, 1971), pp. 603–634.
16. P. Siegel, R. Mose, Ph. Ackerer, and J. Jaffre, "Solution of the Advection-Diffusion Equation Using a Combination of Discontinuous and Mixed Finite Elements," Int. Numer. Methods Fluids **24**, 595–613 (1997).
17. C. Dawson, "High Resolution Upwind-Mixed Finite Element Methods for Advection-Diffusion Equations with Variable Time-Stepping," Numer. Methods Partial Differ. Equations **11**, 525–538 (1995).
18. D. Kuzmin and S. Turek, "Flux Correction Tools for Finite Elements," J. Comput. Phys. **175**, 525–558 (2002).
19. G. I. Marchuk, *Splitting Methods* (Nauka, Moscow, 1988) [in Russian].
20. Ph. Ackerer, A. Younes, and R. Mose, "Modeling Variable Density Flow and Solute Transport in Porous Medium: 1. Numerical Model and Verification," Trans. Porous Media **35**, 345–373 (1999).
21. Y. Achdou, J. Jaffre, D. Svyatski, and Yu. Vassilevski, "Numerical Simulation of Unsteady 3D Flows on Anisotropic Grids," French-Russ. A.M. Lyapunov Inst. Appl. Math. Comput. Sci. Trans. **4**, 107–124 (2003).
22. J.-L. Lions, *Controle optimal de systemes gouvernes par des equations aux derivees partielles* (Gauthier-Villars, Paris, 1968; Mir, Moscow, 1972).
23. I. Kaporin, "High Quality Preconditioning of a General Symmetric Positive Definite Matrix Based on Its UTU + UTR + RTU-Decomposition," Numer. Linear Algebra Appl. **5**, 483–509 (1998).
24. G. Chavent and J. Jaffre, *Mathematical Models and Finite Elements for Reservoir Simulation* (North-Holland, Amsterdam, 1986).
25. H. Hoteit, Ph. Ackerer, and R. Mose, "Etc. New Two-Dimensional Slope Limiters for Discontinuous Galerkin Methods on Arbitrary Meshes," Int. J. Numer. Methods Eng. **61**, 2566–2593 (2004).
26. V. V. Voevodin and Yu. A. Kuznetsov, *Matrices and Computations* (Nauka, Moscow, 1984) [in Russian].
27. J. L. Feike and J. H. Dane, "Analytical Solutions of the One-Dimensional Advection Equation and Two- or Three-Dimensional Dispersion Equation," Water Resour. Res. **26**, 1475–1482 (1990).